

TRANSIENT LAYERS IN THE TOPSIDE IONOSPHERE OF MARS

by

Andrew James Kopf

A thesis submitted in partial fulfillment
of the requirements for the
Master of Science degree in Physics
in the Graduate College of
The University of Iowa

August 2008

Thesis Supervisor: Professor Donald A. Gurnett

Graduate College
The University of Iowa
Iowa City, Iowa

CERTIFICATE OF APPROVAL

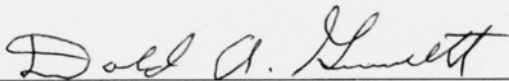
MASTER'S THESIS

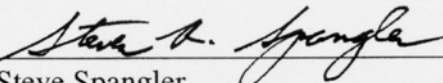
This is to certify that the Master's thesis of

Andrew James Kopf

has been approved by the Examining Committee for the thesis requirement for the Master of Science degree in Physics at the August 2008 graduation.

Thesis Committee:


Donald Gurnett, Thesis Supervisor


Steve Spangler

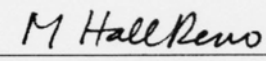

Mary Hall Reno

TABLE OF CONTENTS

LIST OF FIGURES	iii
CHAPTER	
1. MARS EXPRESS AND MARSIS	1
2. SOUNDING THEORY AND MODELING	4
3. TOPSIDE LAYERS	7
4. INTERPRETATION	14
REFERENCES	17

LIST OF FIGURES

Figure

1. The top panel illustrates the frequency dependent reflection of a radar signal from the topside of the Martian ionosphere, and the bottom panel shows the resulting time delay of the reflected signal as a function of frequency. The cusp in the time delay trace at $f_p(\text{max})$ is caused by the very low group velocity and long path length near the peak in the density profile, where $\partial n_e / \partial z = 0$. 5
2. Two ionograms that show the presence of a second layer above the main ionospheric layer. Ionogram (A) has a cusp with a vertex, which indicates the presence of a peak in the density profile, hence a well-defined second layer, at an altitude well above the peak of the main layer. Ionogram (B) has a step without a cusp-shaped vertex, which means that there is a region where $\partial n_e / \partial z$ is near zero, i.e., an inflection point rather than a clearly defined peak in the density profile. 8
3. A spectrogram that shows the transient variations in the electron density of the second layer during a low altitude pass over the ionosphere. The color coding gives the apparent altitude of the reflection, which is the spacecraft altitude minus the apparent range, $c\Delta t/2$. The irregular boundary defined by the cusps and steps gives the maximum electron density of the second layer, $n_e(\text{max}, 2^{\text{nd}} \text{ layer})$. 9
4. A statistical summary of the properties of the second layer. The top panel gives the occurrence probability, the middle panel gives the maximum electron density, and the bottom panel gives the altitude of the maximum computed by inverting equation (2), all as a function of solar zenith angle. The best fit linear function in the last panel shows an upward trend in altitude with increasing solar zenith angle. 11
5. The top panel (A) shows an ionogram with the characteristic signature of a third topside layer. The bottom panel (B) shows the corresponding electron density profile computed by inverting equation (2). The computation was performed assuming a monotonic electron density profile. 12

CHAPTER 1

MARS EXPRESS AND MARSIS

The European Mars Express spacecraft [*Chicarro et al.*, 2004], named for its rapid and streamlined development time, represents ESA's first visit to another planet in the solar system. Mars Express was launched on June 2, 2003, and arrived at Mars less than seven months later, entering orbit on December 25, 2003. Following a series of maneuvers to slow the spacecraft down, Mars Express ultimately settled into a highly elliptical precessing polar orbit. Mars Express completes a full orbit every 6 hours and 43 minutes, with a periapsis altitude of 258 km and an apoapsis of 11,560 km.

The primary objectives of the Mars Express mission were to search for subsurface water (or ice) and to produce global high-resolution photogeology maps. In addition to this, the mission also had a number of secondary objectives. The landing component, Beagle 2, was to study geochemistry and exobiology on the surface of Mars. Unfortunately, Beagle 2 failed to signal following its landing. The orbiting spacecraft also had other objectives, including studying atmospheric circulation, surface-atmosphere interaction, and the subject of this paper, the structure of the ionosphere and its interaction with the interplanetary medium.

In order to accomplish its scientific objectives, the Mars Express orbiting spacecraft carries seven distinct instruments. This paper will focus on one of those instruments, a low-frequency nadir-looking pulse limited radar sounder called the Mars Advanced Radar for Subsurface and Ionosphere Sounding (MARSIS) that is designed to sound the subsurface and ionosphere of Mars [*Picardi et al.*, 2004]. When operating in ionospheric sounding mode, the focus of this paper, MARSIS operates between the periapsis altitude and 1200 km. For

ionospheric sounding, MARSIS transmits a constant frequency radar pulse, which can be stepped through 160 frequencies between 0.1 and 5.4 MHz. The length of this transmitted pulse is a mere 91.43 μ s, which is repeated 130 times per second over each sounding sweep, which lasts 7.38 seconds. As a result, since Mars Express is below 1200 km in altitude for roughly 40 minutes during every orbit, MARSIS can obtain more than 300 direct measurements of the Martian ionosphere per orbit.

Although Mars Express arrived at Mars on December 25, 2003, the MARSIS antennae were not deployed until roughly a year and a half later. Due to severe mass limitations, MARSIS antennae are a new type, a folding fiberglass tube roughly 3.8 cm in diameter which supports wires that form the conductive element of the antennae. All three components of the antenna system, two 20-meter dipole antennae and one 7-meter clutter-cancelling monopole antenna, were launched in a folded position against the spacecraft, designed to self-deploy under the control of three pyrotechnic release mechanisms. Fears that this deployment strategy could result in the antennae striking and damaging the spacecraft forced the antennae deployment to wait until the other primary science mission objectives had been completed. After roughly an 18 month wait, the first dipole antenna was successfully deployed on May 10, 2005, the second followed suit on June 14, 2005, and the monopole antenna completed the deployment operation on June 17, 2005. MARSIS subsequently began normal operation on July 4, 2005.

Spacecraft radar sounders, developed in the 1960s to study Earth's ionosphere [Calvert, 1966], have proven to be a powerful tool for studying planetary ionospheres. Before MARSIS, most knowledge of the Martian ionosphere came from radio occultation measurements [Zhang *et al.*, 1990; Pätzold *et al.*, 2005]. The MARSIS data nicely

complement the radio occultation measurements by providing better spatial resolution and the ability to explore regions, for example at high altitudes and near the subsolar point, where radio occultations cannot be performed. In an overview of the early MARSIS ionospheric sounding results *Gurnett et al.* [2008] discussed the existence of a second layer in the ionosphere at an altitude of about 200 km, well above the main photo-ionization layer, which occurs at about 120 to 140 km [*Morgan et al.*, 2008]. In this paper I present a study of this second layer, and report the discovery of a third layer.

CHAPTER 2

SOUNDING THEORY AND MODELING

Before discussing the new results, it is useful to give a brief review of ionospheric radar sounding. A horizontally stratified ionosphere provides a nearly perfect reflecting surface for radar sounding. The radar pulse cannot propagate at frequencies below the plasma frequency, given by

$$f_p = 8980 \sqrt{n_e} \text{ Hz}, \quad (1)$$

where n_e is the electron density in cm^{-3} [Gurnett and Bhattacharjee, 2005]. The pulse is therefore reflected as soon as it reaches the altitude where the wave frequency equals the plasma frequency. For frequencies above the maximum plasma frequency, the radar pulse passes through the ionosphere and is reflected from the surface of the planet as illustrated in the top panel of Figure 1.

Ionospheric sounding data are usually displayed as an ionogram, which is a plot of the reflected radio wave intensity as a function of the transmitted frequency and the time delay of the received radar echo. A sketch of the ionospheric and surface reflection trace expected in a typical ionogram is shown in the bottom panel of Figure 1. The scale on the left is the time delay, Δt , plotted positive downward. The scale on the right, called “apparent range,” is the distance to the reflection point, $c\Delta t/2$, computed assuming that the radar pulse travels at the speed of light, c . The maximum plasma frequency in the ionosphere, $f_p(\text{max})$, can be identified from the discontinuity in the echo trace labeled “cusp”. The vertex of the cusp, which defines the boundary between the ionospheric and ground reflection traces, is caused by the long time delays that occur as the wave propagates through the relatively extended region where the wave frequency is very close to the maximum plasma frequency.

A-D08-080-2

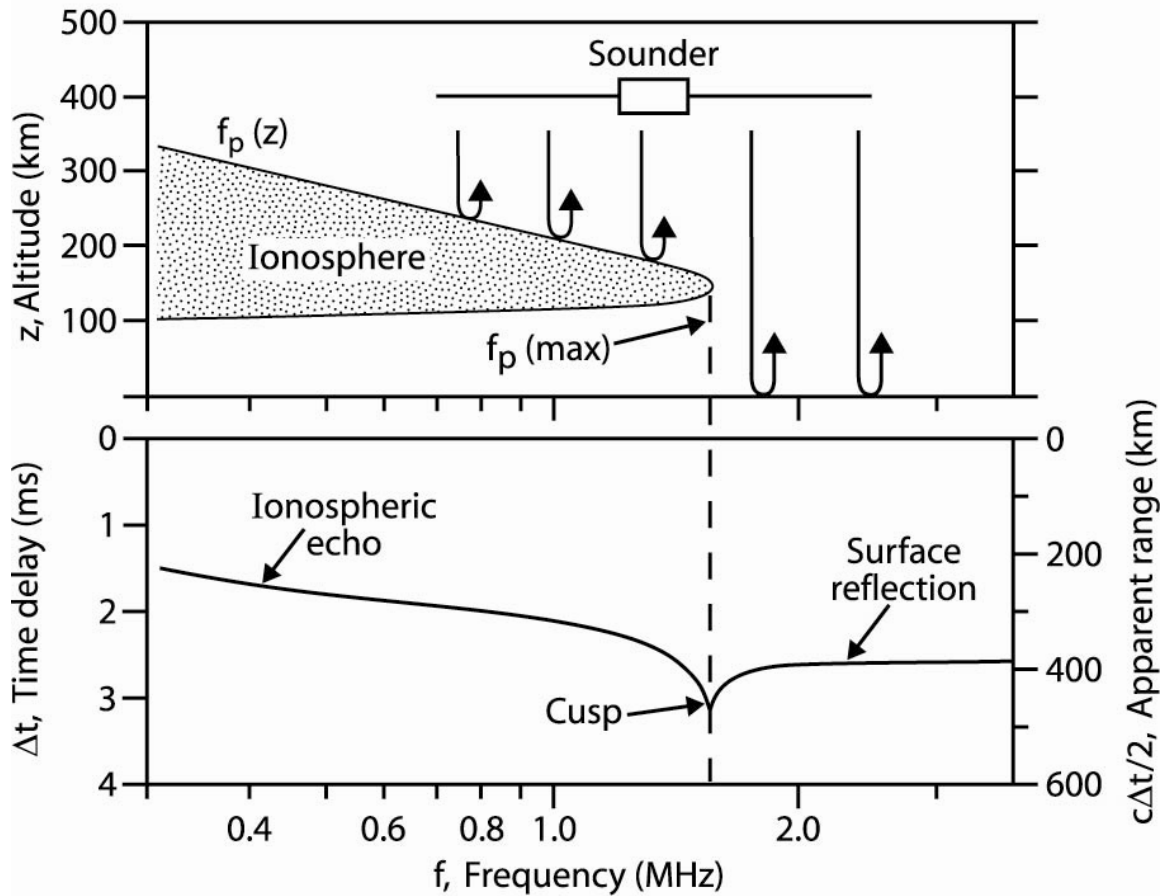


Figure 1

Figure 1. The top panel illustrates the frequency dependent reflection of a radar signal from the topside of the Martian ionosphere, and the bottom panel shows the resulting time delay of the reflected signal as a function of frequency. The cusp in the time delay trace at $f_p(\text{max})$ is caused by the very low group velocity and long path length near the peak in the density profile, where $\partial n_e/\partial z = 0$.

Cusps occur whenever the electron density has a local maximum, i.e., when $\partial n_e/\partial z = 0$, see Budden [1961]. If the surface reflection is too weak to detect, then only the ionospheric half of the cusp can be detected. This condition often occurs at solar zenith angles (SZA) less than about 60° and during solar energetic particle events [Morgan et al., 2006].

Although the apparent range gives a rough estimate of the distance to the reflection point, for accurate measurements the deviation from the speed of light caused by the ionospheric plasma must be taken into account. Assuming vertical reflection from a horizontally stratified ionosphere, it can be shown that the time delay as a function of frequency is given by

$$\Delta t(f) = \frac{2}{c} \int_{z(f_p)}^{z_{sc}} \frac{dz}{\sqrt{1 - (f_p(z)/f)^2}}, \quad (2)$$

where z_{sc} is the altitude of the spacecraft and $z(f_p)$ is the altitude of the reflection point [Gurnett *et al.*, 2005]. If the electron density is assumed to be a monotonic function of altitude, then the measured time delay as a function of frequency, $\Delta t(f)$, can be inverted to give the plasma frequency (or electron density) as a function of altitude, $f_p(z)$, see *Budden* [1961]. Because of the monotonic requirement, a unique inversion cannot be obtained if there are distinct layers separated by points where $\partial n_e / \partial z = 0$, although limits can be put on such inversions.

Once the inversion has been completed, the resulting data can be fit to a theoretical model to yield a physical result. An appropriate model for these physical circumstances, which has been used for the following analysis, was derived by *Chapman* [1931]

$$n_e = n_0 \exp \left[\frac{1}{2} \left\{ 1 - \frac{z - z_0}{H} - \text{Ch}(x, \chi) \exp \left(-\frac{z - z_0}{H} \right) \right\} \right] \quad (3)$$

where z is the altitude, H is the scale height of the neutral atmosphere, n_0 is the maximum electron density at the subsolar point, and z_0 is the altitude of this maximum. The function $\text{Ch}(x, \chi)$ is Chapman's grazing incidence function, which takes into account absorption of the solar radiation as it passes obliquely through the atmosphere. This function depends on the solar zenith angle χ and the parameter $x = (R + z_0)/H$, where R is the radius of Mars.

CHAPTER 3

TOPSIDE LAYERS

In addition to the cusp associated with the main ionospheric layer, many MARSIS ionograms also have a second cusp at a substantially lower frequency, indicating the presence of a second layer well above the main ionospheric layer. An example of an ionogram with such a second cusp is shown in Figure 2A. The maximum plasma frequency (hence electron density) of the second layer is given by the frequency at the vertex of the cusp, 1.65 MHz in this case, which using equation (1) corresponds to an electron density of $3.37 \times 10^4 \text{ cm}^{-3}$ at the peak of the second layer. Sometimes the vertex of the cusp is missing and the second layer can only be identified by a distinct downward step in the trace with increasing frequency, as in Figure 2B.

Inspection of many such examples reveals that the maximum electron density of the second layer is highly variable. To illustrate this variability, Figure 3 shows a color-coded plot of the apparent altitude of the ionospheric reflection as a function of electron density and time for a typical dayside pass. (Apparent altitude is defined as the spacecraft altitude minus the apparent range, i.e., $z = z_{sc} - c\Delta t/2$, where z_{sc} is the spacecraft altitude.) The scale on the right is the frequency of the sounding pulse, and the scale on the left is the corresponding electron density. The peak density of the second layer, $n_e(\text{max, main layer})$, can be identified from the irregular boundary defined by the isolated cusps (usually green) and downward steps (usually from red to yellow) in the apparent altitude. As can be seen the boundary not only fluctuates considerably, from about $(2 \text{ to } 5) \times 10^4 \text{ cm}^{-3}$, but also disappears completely at times, indicating that the second layer is a transient phenomenon. The time scale of the fluctuations varies considerably, from tens of seconds to several minutes, corresponding to

A-D08-078-2

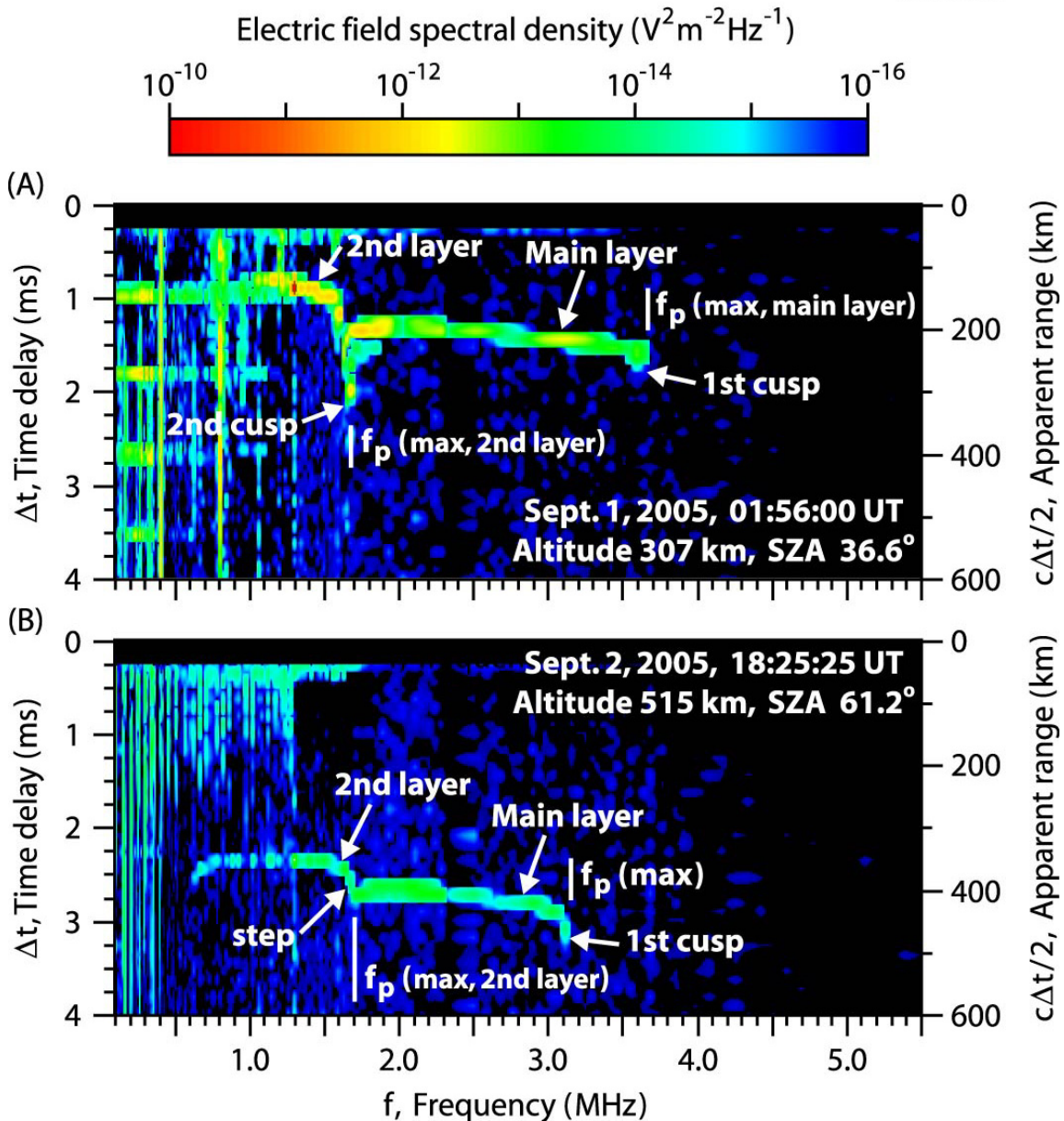


Figure 2

Figure 2. Two ionograms that show the presence of a second layer above the main ionospheric layer. Ionogram (A) has a cusp with a vertex, which indicates the presence of a peak in the density profile, hence a well-defined second layer, at an altitude well above the peak of the main layer. Ionogram (B) has a step without a cusp-shaped vertex, which means that there is a region where $\partial n_e/\partial z$ is near zero, i.e., an inflection point rather than a clearly defined peak in the density profile.

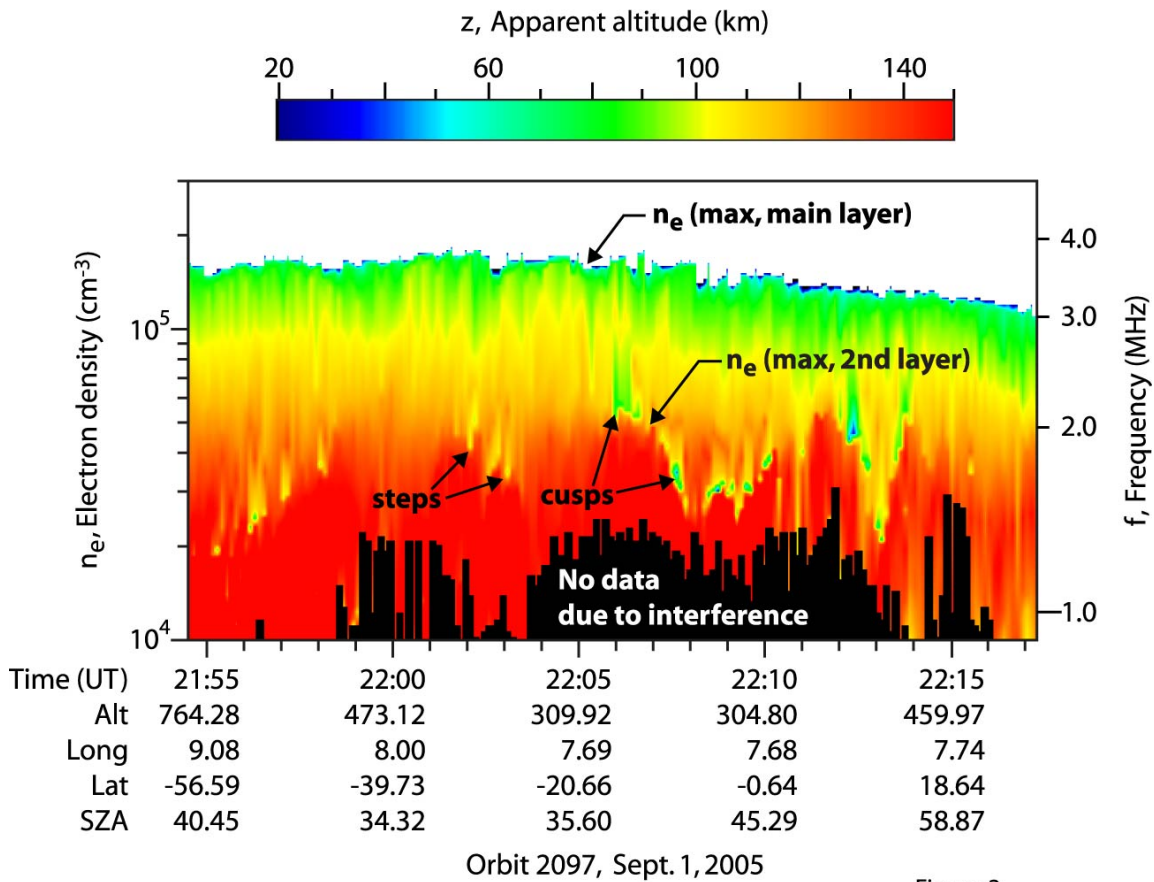


Figure 3

Figure 3. A spectrogram that shows the transient variations in the electron density of the second layer during a low altitude pass over the ionosphere. The color coding gives the apparent altitude of the reflection, which is the spacecraft altitude minus the apparent range, $c\Delta t/2$. The irregular boundary defined by the cusps and steps gives the maximum electron density of the second layer, $n_e(\text{max}, 2^{\text{nd}} \text{ layer})$.

horizontal spatial scales ranging from a few tens to several hundred km. These fluctuations are in sharp contrast to the maximum electron density of the main layer, $n_e(\text{max}, \text{main layer})$, which is relatively smooth and continuous during the entire pass. The transient layers are observed on nearly every dayside pass.

To study the statistical properties of the second layer, approximately 1500 ionograms have been analyzed for all of the orbits during the period from August 5, 2005, to September

5, 2005. These orbits cover a wide range of latitudes and longitudes, and solar zenith angles from near the subsolar point ($SZA = 0^\circ$) to the terminator ($SZA = 90^\circ$). Figure 4 shows the probability of occurrence, the maximum electron density, and the altitude of the second layer, all as a function of solar zenith angle. The probability of occurrence has a broad maximum of about 60% near the subsolar point and decreases with increasing solar zenith angle to less than 5% at the terminator. The maximum electron density of the second layer ranges from about $(2 \text{ to } 7) \times 10^4 \text{ cm}^{-3}$ and the altitude of the maximum density varies from about 180 to 220 km, with an average of about 200 km. There is a slight tendency for the maximum electron density to decrease, and the altitude of the maximum to increase, with increasing solar zenith angle. The occurrence probability shows no relationship to surface features, or to the crustal magnetic fields discovered by *Acuña et al.* [1999]. Also, there is no obvious relationship to variations in the solar EUV radiation as monitored via the F10.7 solar radio flux, or to solar energetic particle events.

Figure 5A shows an ionogram with a third cusp (or step) indicating the presence of a third layer above a rather well defined second layer. For this case the electron density profile has been computed by inverting equation (2). The resulting profile is shown in Figure 5B. Since the presence of the topside layers leads to an indeterminacy in the inversion process, I have rather arbitrarily assumed that the electron density profile is a continuous monotonic function across the interface between each of the layers. This assumption gives an upper altitude limit to the true profile. The resulting inversion places the peak of the main layer at an altitude of 138 km with a maximum density of $n_e(\text{max}) = 1.66 \times 10^5 \text{ cm}^{-3}$. These parameters are very close to the nominal values given by *Morgan et al.* [2008] for the main layer at this solar zenith angle ($SZA = 31.9^\circ$).

A-D08-068-5

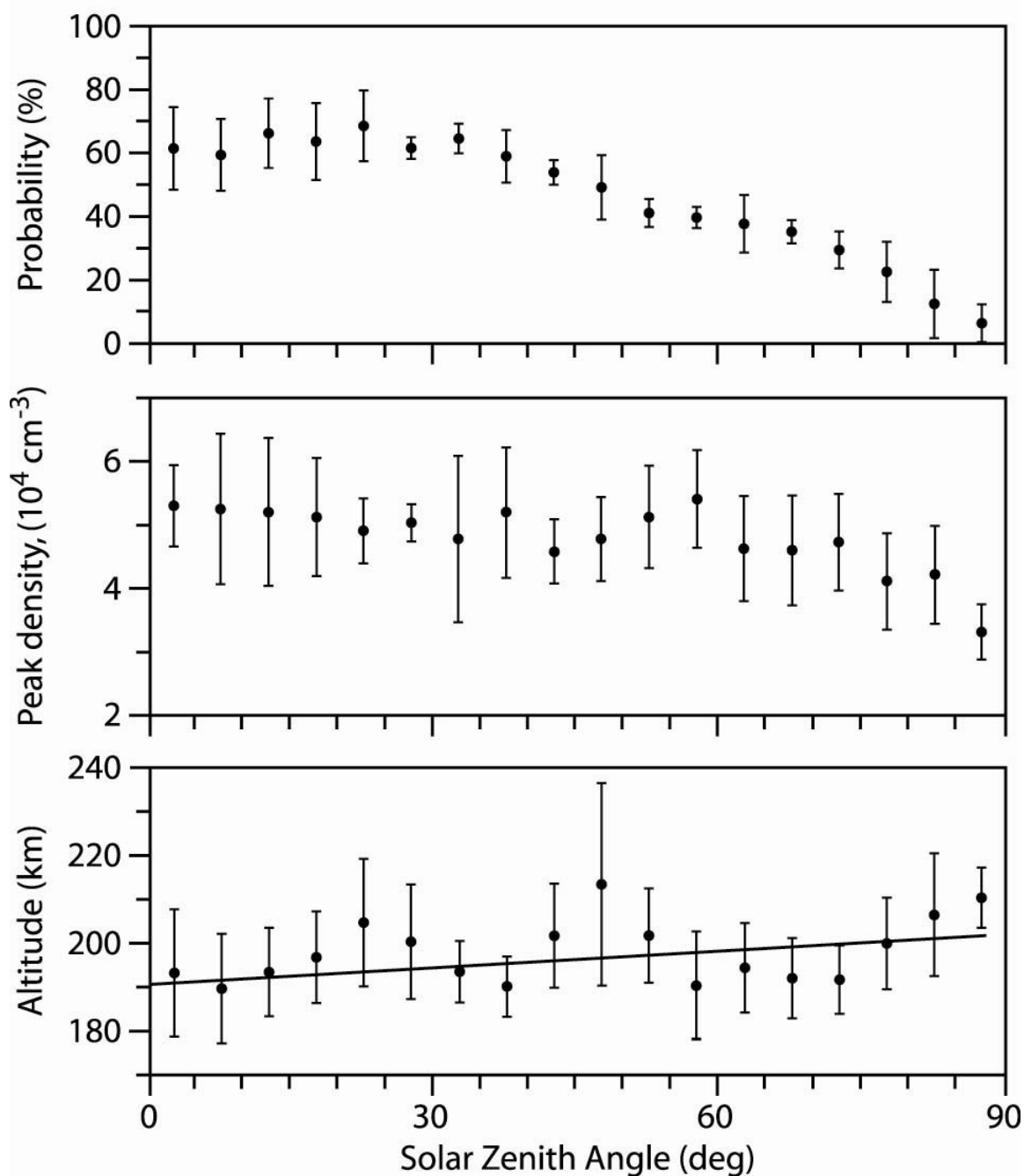


Figure 4

Figure 4. A statistical summary of the properties of the second layer. The top panel gives the occurrence probability, the middle panel gives the maximum electron density, and the bottom panel gives the altitude of the maximum computed by inverting equation (2), all as a function of solar zenith angle. The best fit linear function in the last panel shows an upward trend in altitude with increasing solar zenith angle.

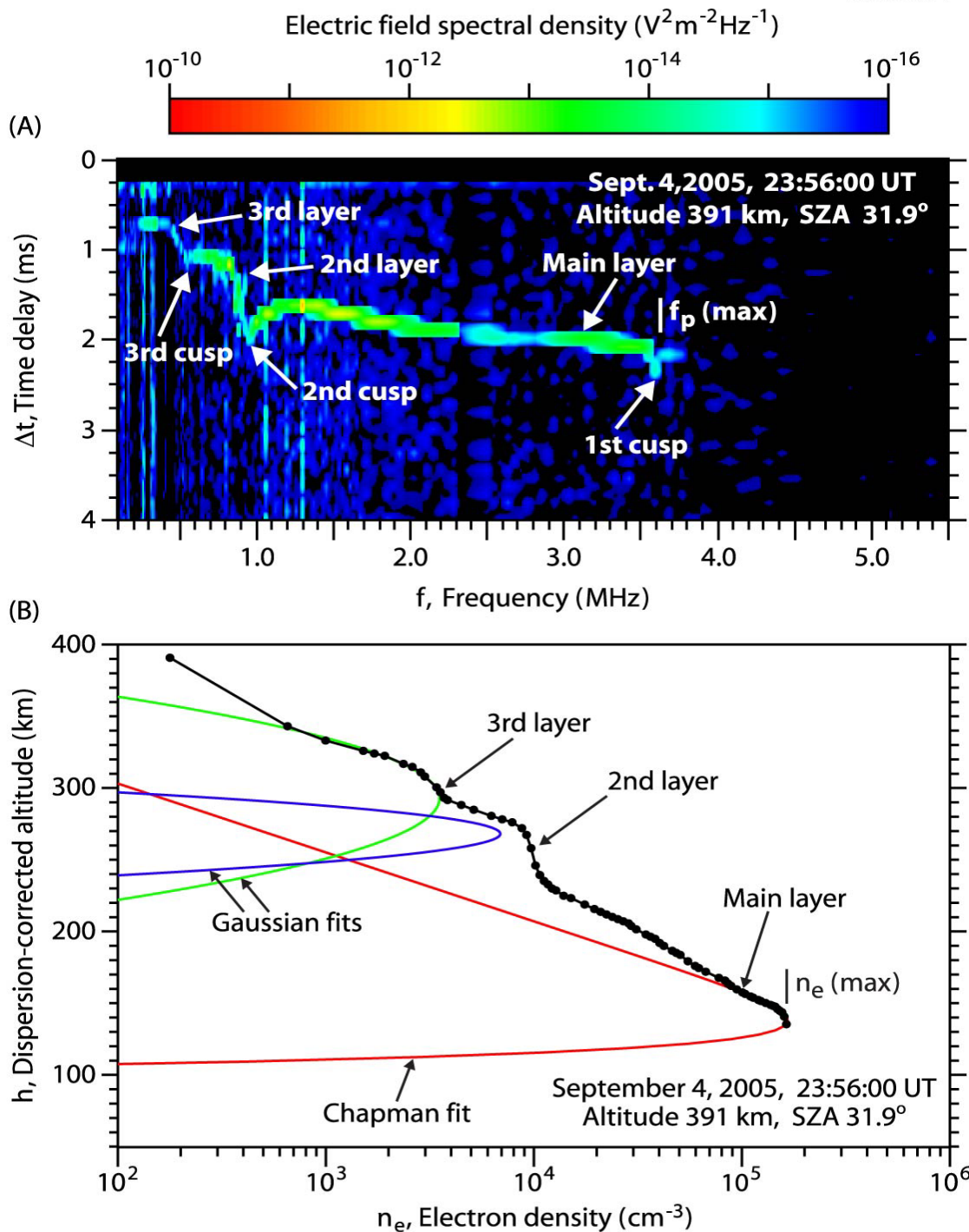


Figure 5

Figure 5. The top panel (A) shows an ionogram with the characteristic signature of a third topside layer. The bottom panel (B) shows the corresponding electron density profile computed by inverting equation (2). The computation was performed assuming a monotonic electron density profile.

This good agreement with previous results gives us confidence that the computed profile is reasonably close to the true profile. The red line shows a fit to the Chapman photo-equilibrium equation [*Chapman*, 1931] for the main layer, and the blue and green lines show Gaussian fits to the electron density profile for the second and third layers. The vertical total electron content (TEC) for the main, second, and third layers are 7.17×10^{11} , 1.72×10^{10} , and $2.34 \times 10^{10} \text{ cm}^{-2}$, respectively. These TEC values show that the total number of electrons involved in the topside layers is quite small, ~6%, compared to the main layer. Third layers of the type shown in Figure 5 are quite rare and only occur about 1% of the time. As with the second layer, they are also highly transient.

CHAPTER 4

INTERPRETATION

When the second layer was first discovered, this feature was believed to be possibly related to the O^+ layer discovered by Viking [*Hansen et al.*, 1977] at an altitude of about 225 km. However, the vertical thickness of the O^+ layer discovered by Viking, about 100 km, appeared to be too large to account for the discrete topside layers detected by MARSIS, which have vertical thicknesses of only a few tens of km (see Figure 5). Also, since the O^+ production is an equilibrium process, there is no way that such a process could account for the highly transient behavior of the topside layers. Instead, the transient behavior is indicative of some dynamical process in the upper ionosphere of Mars. Recently, local electron density measurements reported by *Duru et al.* [2008] from electron plasma oscillations excited by the MARSIS sounder have shown that at altitudes above 275 km the electron density is highly variable, with fluctuations often exceeding 25% in the range from 300 to 350 km, and even larger at higher altitudes. The transient topside layers detected by the MARSIS radar soundings are most likely just another manifestation of these same fluctuations.

Several possibilities exist for exciting such fluctuations. *Wang and Nielson* [2002] have suggested that fluctuations in the solar wind ram pressure could excite large amplitude magnetohydrodynamic waves in the upper levels of the ionosphere, especially near the subsolar point where the solar wind pressure variations are the largest. Indeed such waves have been observed in radio occultation data [*Wang and Nielsen*, 2003] at altitudes from about 145 to 200 km. Since nonlinearities often cause large amplitude waves to curl over and break, like water waves at a beach, it is possible that such structures could appear as

distinct layers to a radar sounder. The dayside source of these waves would be consistent with the observed solar zenith angle dependence of the transient topside layers, which occur most frequently near the subsolar point. However, it is not clear that the solar wind pressure fluctuations occur with sufficient amplitude and over the very broad range of time scales needed to explain the near continuous presence of the transient topside layers.

Because of the velocity shear that exists between the solar wind and the ionosphere of an unmagnetized planet, various researchers have also suggested that large amplitude waves could be generated in the upper levels of the ionosphere via the Kelvin-Helmholtz instability, see for example *Terada et al.* [2002]. *Penz et al.* [2004] have argued that large amplitude waves generated via the Kelvin-Helmholtz instability could play an important role in the loss of ions from the upper ionosphere of Mars. Since Kelvin-Helmholtz waves are known to evolve into nonlinear structures with a curl-over and to form detached plasma clouds, it is possible that such structures could appear as distinct layers to a radar sounder. However, the Kelvin-Helmholtz mechanism is expected to be most unstable near the terminator, where the velocity shear is large, and may very well be stable near the subsolar point where the velocity shear is small. This trend is in disagreement with the solar zenith angle dependence in Figure 4, although further study is needed to see if this disagreement is sufficiently serious to completely rule out the Kelvin-Helmholtz mechanism.

In addition to nonlinear wave mechanisms there are almost certainly other solar wind related processes that could affect the density in the upper levels of the ionosphere. For example, magnetic reconnection near the nose of the induced magnetosphere could lead to the enhanced transport of plasma out of the ionosphere [*Eastwood et al.*, 2008]. Also, it has been shown that the $\mathbf{v} \times \mathbf{B}$ electric field associated with the bulk motion of the solar wind can

cause plasma loss by accelerating ions upward out of the ionosphere [*Modolo et al.*, 2005]. One unusual effect that has been observed is that the cusps or steps in the ionograms appear to be caused more by an erosion of the plasma density in the upper levels of the main layer rather than by an enhancement in the density of the second layer. This effect can be seen in Figure 3, where the apparent altitude of the second layer (red) remains nearly constant, whereas the apparent altitudes of the upper levels of the main layer (usually yellow or green) show sharp irregular decreases. Clearly, further study is needed to determine which, if any, of the above processes are involved in the formation of the topside layers.

REFERENCES

- Acuña, M. H., et al. (1999), Global distribution of crustal magnetization discovered by the Mars Global Surveyor MAG/ER experiment, *Science*, 284, 790-793.
- Budden, K. G. (1961) *Radio Waves in the Ionosphere*, Cambridge Univ. Press, Cambridge, 160-162.
- Calvert, W. (1966), Ionospheric topside soundings. *Science*, 154, 228-234.
- Chapman, S. (1931), The absorption and dissociative or ionizing effect of monochromatic radiation in an atmosphere on a rotating Earth, Part II. Grazing incidence, *Proc. Roy. Soc. London*, 43, 483-501, doi:10.1088/0959-5309/43/5/302.
- Chicarro, A., P. Martin, and R. Traunter (2004), The Mars Express mission: An overview, in *Mars Express: A European Mission to the Red Planet*, Eur. Space Agency Spec. Publ. SP-1240, 3-16.
- Duru, F., D. A. Gurnett, D. D. Morgan, R. Modolo, A. F. Nagy, and D. Najib (2008), Electron densities in the upper ionosphere of Mars from the excitation of electron plasma oscillations, *J. Geophys. Res.*, in press.
- Eastwood, J. P., D. A. Brain, J. S. Halekas, J. F. Drake, T. D. Phan, M. Øieroset, D. L. Mitchell, R. P. Lin, and M. Acuña (2008), Evidence for collisionless magnetic reconnection at Mars, *Geophys. Res. Lett.*, 35, L02106, doi:10.1029/2007GL032289.
- Gurnett, D. A. and A. Bhattacharjee (2005), *Introduction to Plasma Physics*, Cambridge Univ. Press, Cambridge, UK, 11.
- Gurnett, D. A., et al. (2005), Radar soundings of the ionosphere of Mars, *Science*, 310, 1929-1933, doi:10.1126/science.1121868.
- Gurnett, D. A., et al. (2008), An overview of radar soundings of the Martian ionosphere from the Mars Express spacecraft, *Adv. Space Research*, 41, 1335-1346, doi:10.1016/j.asr.2007.01.062.
- Hanson, W. B., S. Sanatani, and D. R. Zuccaro (1977), The Martian ionosphere as observed by the Viking retarding potential analyzers, *J. Geophys. Res.*, 82(28), 4351-4363.
- Modolo, R., G. M. Chanteur, E. Dubinin, and A. P. Matthews (2005), Influence of the solar EUV flux on the Martian plasma environment, *Annales Geophys.*, 23, 433-444.
- Morgan, D. D., D. A. Gurnett, D. L. Kirchner, R. L. Huff, D. A. Brain, W. V. Boynton, M. H. Acuna, J. J. Plaut, and G. Picardi (2006), Solar control of radar wave absorption by the Martian ionosphere, *Geophys. Res. Lett.*, 33, L13202, doi:10.1029/2006GL026637.

Morgan, D. D., D. A. Gurnett, D. L. Kirchner, J. L. Fox, E. Nielson, and J. J. Plaut (2008), Variation of the Martian ionospheric electron density from Mars Express radar soundings, *J. Geophys. Res.*, in press.

Pätzold, M., S. Tellmann, B. Häusler, D. Hinson, R. Schaa, and G. L. Tyler (2005), A sporadic third layer in the ionosphere of Mars, *Science*, *310*, 837-839.

Penz, T., et al. (2004), Ion loss on Mars caused by the Kelvin-Helmholtz instability, *Planetary and Space Sci.*, *52*, 1157-1167.

Picardi, G., et al. (2004), MARSIS: Mars advanced radar for subsurface and ionosphere sounding, in *Mars Express: A European Mission to the Red Planet*, *Eur. Space Agency Spec. Publ. SP-1240*, 51-70.

Terada, N., S. Machida, and H. Shinagawa (2004), Global hybrid simulation of the Kelvin-Helmholtz instability at the Venus ionopause, *J. Geophys. Res.*, *107*, 1471, doi:1029/201JA009224.

Wang, J.-S. and E. Nielsen (2002), Dispersion relation and numerical simulation of hydrodynamic waves in Mars' topside ionosphere, paper presented at the 27th General Assembly of the European Geophysical Society, Nice, France.

Wang, J.-S., and E. Nielsen (2003), Wavelike structures in the Martian topside ionosphere observed by Mars Global Surveyor, *J. Geophys. Res.*, *108*(E7), 5078, doi:1029/2003JE002078.

Zhang, M. G. H., J. G. Luhmann, and A. J. Kliore (1990), A post Pioneer Venus reassessment of the Martian dayside ionosphere as observed by radio occultation methods, *J. Geophys. Res.*, *95*, 14,829-14,839.